Proceedings of the
Annual Stability Conference
Structural Stability Research Council
Atlanta, Georgia, April 21-24, 2026

Probabilistic Stability Assessment of Metal Building Roof Corners Under Tornado-Induced Wind Loads

Shihang Wang[1], Xinyang Wu[2], Delong Zuo[3], Hannah B. Blum[4]

Abstract

Metal building systems are commonly used for warehouses, schools and shelters in rural communities, where their low cost, ease of construction and adaptable structural layouts make them a practical choice. However, these systems are vulnerable to tornado-induced wind loads, particularly at roof corner regions, where intensified uplift pressures due to turbulent airflow frequently result in fastener-related failures that compromise the roof panel's integrity.

This study investigates the role of fasteners in governing the load-carrying performance under tornado-induced wind loads, with a focus on how localized fastener failure can trigger broader panel deformation and reduce overall buckling resistance. A detailed shell finite element model representing the corner section of a metal building was developed in ABAQUS. The model incorporates material and geometric nonlinearity, as well as standing-seam roof and upper frame details. Connector elements are modeled with defined pull-out and shear capacities, enabling the simulation of both local fastener failure and its impact on panel buckling.

Building on the prior mid one-bay span model focused on the buckling of roof panel and secondary members, the corner model now also captures fastener failure. By applying both external and internal wind pressures obtained from tornado simulator experiments, the analysis captures the sequence and distribution of fastener failures and their influence on panel buckling, uplift, and overall instability under four different loading conditions. The number and percentage of failed fasteners are used to quantify damage states and provide insight into the progression of roof panel buckling and failure.

1. Introduction

Metal building systems are widely employed for low-rise facilities due to their cost-effectiveness, rapid construction, and flexible layouts. Conversely, their light framing and thin steel roof panels can be sensitive to tornado winds. Unlike steady straight-line winds, tornado loading changes

[1]Graduate Research Assistant, University of Wisconsin-Madison, <swang2378@wisc.edu>;
[2]Graduate Research Assistant, Texas Tech University , <xinyawu@ttu.edu>;
[3]Professor, Texas Tech University, <delong.zuo@ttu.edu>;
[4]Alain H. Peyrot Associate Professor, University of Wisconsin-Madison, <hannah.blum@wisc.edu>

rapidly in time and space, creating intense uplift load on roof surfaces (Roueche, Prevatt, and Haan, 2020; Sengupta et al., 2008; Kopp and Wu, 2020). Roof corners are especially vulnerable. The airflow near edges and corners can produce the highest suction load, often making connections the weak link in these scenarios (Haan, Balaramudu, and Sarkar, 2010; Marshall, 2004). Such failures can compromise the stability of the entire roof system, even if the main framing members have not yet reached their strength limits (Xia, Kopp, and Chen, 2023).

In authors' previous work (Wang et al., 2025), tornado simulator pressure time histories were applied to a detailed shell finite element submodel to study middle roof panel and secondary member buckling under transient wind loading. While that study improved understanding of buckling behavior in the mid-roof region, but it did not focus on the roof corner region or capture fastener level failure mechanisms. Consequently, the initiation and propagation of connection failures in the corner zones, as well as their coupling with uplift deformation and structural instability, remain insufficiently defined.

This study addresses these gaps by developing a high fidelity shell finite element submodel of a metal building roof corner in ABAQUS (Abaqus, 2016) that includes material and geometric nonlinearity and represents clips and eave screws as discrete connectors with pull-out and shear failure. To investigate the influence of different opening conditions, tornado simulator net pressure time histories are applied under four configurations at reference tornado wind speeds of 30, 40, 50, 60, and 70 m/s. For each configuration and reference wind speed, 25 simulations are conducted using independent net pressure records to support a probabilistic assessment by evaluating the final percentage of failed fasteners. Additionally, representative simulations are analyzed to document deformation patterns and failure locations, specifically to demonstrate how opening conditions alter internal pressures and modify the overall structural behavior.

2. Laboratory measurement of tornado loading

The wind loading used in this study comes from laboratory measurements obtained at the Texas Tech University tornado simulator. The simulator produces a translating, laboratory scale tornado that traverses a scaled building model instrumented with synchronized external and internal pressure taps (shown in Fig.1). Detailed descriptions of the simulator, pressure tap layout, and pressure load calculation are provided in the authors' previous work (Wang et al., 2025).

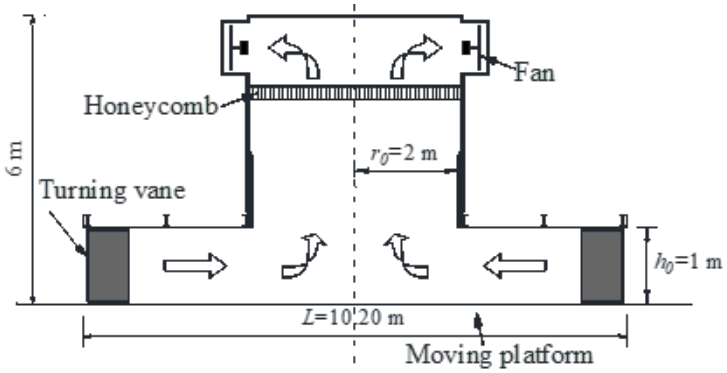

Figure 1: A schematic drawing of VorTECH

In this work, the external and internal pressure time histories were combined to form net pressure on the roof panel and applied over the full duration of each tornado record. Pressure coefficients were converted to physical pressure (p) using Eq. 1:

$$p = C_{p\_net} \times 0.5\rho \left(V_{ref}\right)^2 \tag{1}$$

where $C_{p,\text{net}}$ is the measured net pressure coefficient time history, V_{ref} reference tornado wind speed defined as the maximum mean tangential velocity for the record, and ρ is the air density.

Four internal pressure configurations were considered to represent enclosed and opening conditions on the metal building system (Fig.2). Configuration 1 includes only background leakage, meaning no additional openings are created during the experiment. Configuration 2 i ncludes background leakage plus a permanent door opening, where an additional door opening is present and remains open for the entire record. Configuration 3 includes background leakage plus a sudden door opening during the record, with the door opened at $x/r_c = \pm 0.5$ (defined in Fig.3). Configuration 4 is the same sudden opening case, but with the door opened at $x/r_c = \pm 1$. Here r_c is the core radius of the vortex. Table 1 summarizes the experimental configurations, which influence the internal pressure and therefore affects the net roof uplift applied to the corner submodel.

Table 1: Configurations

Configuration	Description
1	background leakage
2	background leakage + permanent opening
3	background leakage + sudden opening at $x/r_c = \pm 0.5$
4	background leakage + sudden opening at $x/r_c = \pm 1$

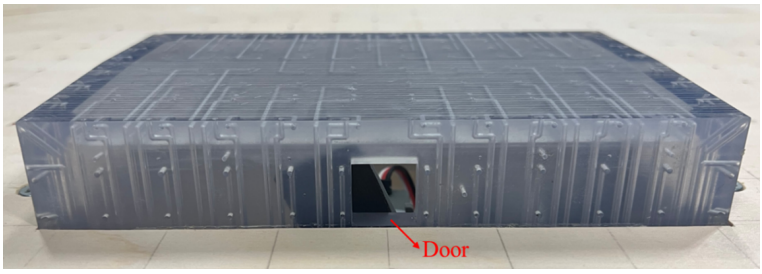

Figure 2: Building model and opening position

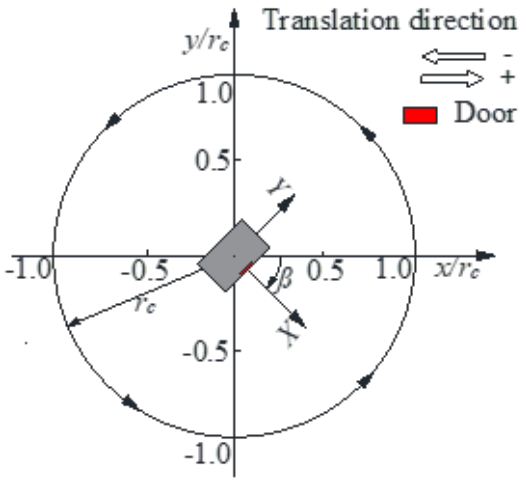

Figure 3: Experiment configuration

3. Finite element modeling

A detailed ABAQUS finite element submodel of the roof corner region (shown in Fig. 4) was developed to capture the coupled response of roof panels, secondary framing, and connection behavior under tornado-induced uplift. The submodel spans from the endwall line to the adjacent interior frame line and covers half of a bay, with overall plan dimensions of 40 ft by 36 ft. The assembly includes the end wall framing components (rake angle and rake support), eave member, purlins, sag angles, two rafter segments, and standing-seam roof panels assembly connected by clips and eave screws.

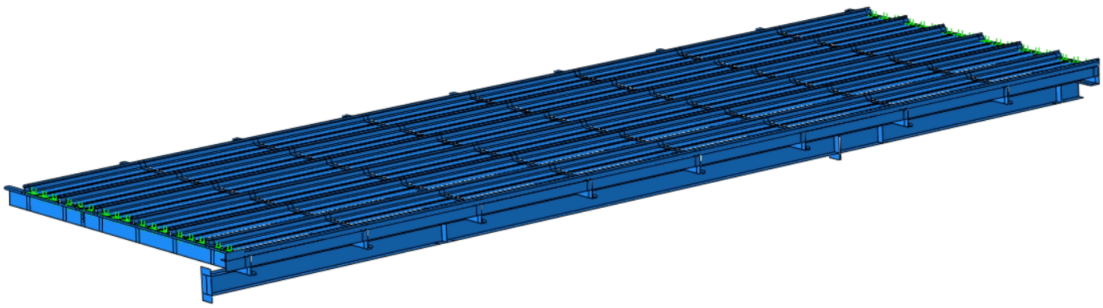

Figure 4: roof corner submodel

3.1 Components properties

All structural components in the roof corner submodel were modeled using S4R shell elements in ABAQUS, consistent with prior finite element studies of metal building systems (Yu and Schafer, 2006; Bajwa, 2010; Hong, 2007; Niari, Rafezy, and Abedi, 2015; Kim, 2010). Material type and thickness for each part are summarized in Table 2. Unless noted otherwise, material modeling and member interactions follow the authors' previous middle roof one bay model (Wang et al., 2025).

Table 2: Material and thickness on parts

Part name	Material	Thickness (in)
Rafter-Flange	HRS	0.125
Rafter-Web	HRS	0.250
Rafter-Splice	HRS	0.375
Eave	CFS	0.100
Purlin	CFS	0.075
Rake angle	CFS	0.075
Rake support	CFS	0.075
Roof panel	CFS	0.030
Sag angle	HRS	0.125

The mesh sizes for the roof corner submodel are summarized in Table 3.

Table 3: Mesh size in dynamic analysis

Part name	Mesh Size (in)
Rafter	1.4
Eave	1.4
Purlin	1.4
Rake angle	1.4
Rake support	1.4
Sag angle	1.4
Roof panel	1

3.2 Fastener and connection modeling

Fasteners were modeled using connector elements with prescribed pull-out and shear capacities to capture localized fastener failure and its interaction with roof-panel uplift deformation. Clip properties were derived from uplift test results reported by Sinno (Sinno, 2005), where static tests were conducted in accordance with ASTM E1592, and were supplemented with manufacturer provided values where needed. Screw parameters were provided by SFS Group USA, Inc (SFS Group USA, Inc., 2024).

Clips attach the standing-seam panel ribs to the purlin top flanges. The connector kinematics are defined to permit relative sliding along the seam axis while restraining the remaining translational degrees of freedom, consistent with typical standing-seam clip behavior. This sliding displacement is limited to 1.25 in to represent the physical slot length. A nominal penalty stiffness is assigned in the sliding direction to simulate frictional resistance and enhance numerical stability. Eave screws connect the roof panel to the eave member. For both clips and screws, failure is simulated by deactivating the connector element once it exceeds its defined pull-out or shear capacity. The accumulation of failed fasteners is tracked throughout the analysis to quantify the progression of damage.

3.3 Boundary conditions

Fixed boundary conditions were applied to the rafter ends at the rafter-to-column interface. The endwall edge of the roof panel was supported by the rake angle and rake support assembly, which was tied to the rafter upper flange. Symmetry constraints were applied along cut boundaries of purlins and roof panels by restricting displacement normal to the cut plane.

3.4 Dynamic analysis setup and tornado load applied

Dynamic analyses were performed in ABAQUS/Explicit following the same solution strategy, step setup, and numerical controls as the previous study (Wang et al., 2025). The key difference in the present work is the clip and screw connectors with pull-out/shear failure, which enables tracking of fastener failure progression. The measured external and internal pressure time histories are mapped to the roof panel surfaces and applied as transient surface pressures. The 40 ft panel length was divided into four equal segments, and the six roof panels in the transverse direction were divided into two groups. This partitioning results in a total of eight loading zones, each assigned a corresponding time-varying pressure history. Reference wind speeds range from 30 to 70 m/s, covering scenarios from minor damage to widespread connection loss. Mass scaling was used to improve computational efficiency while maintaining a quasi-static response.

4. Results

Results are summarized using the average final percentage of failed fasteners across 25 runs for each configuration at each reference wind speed. Deformed shapes and failure location plots are shown for a representative record whose final fasteners failure percentage is closest to the ensemble median.

Across all internal pressure configurations, the final percentage of failed fasteners increases with reference wind speed. At 30 m/s, failures are isolated and the roof corner response shows limited out of plane deformation. At 50, 60, and 70 m/s, connection loss extends across a large portion of the corner region and the roof panel develops large uplift deformation. Because the low speed regime has limited damage and the high speed regime has widespread connection loss, configuration effects are most clearly interpreted at 40 m/s, where failures develop without overwhelming the entire corner. Fig. 5a and Fig. 5b provide representative deformed shapes at low and high wind speeds to illustrate the contrast between a fully restrained roof corner response and a roof panel with extensive fastener failure.

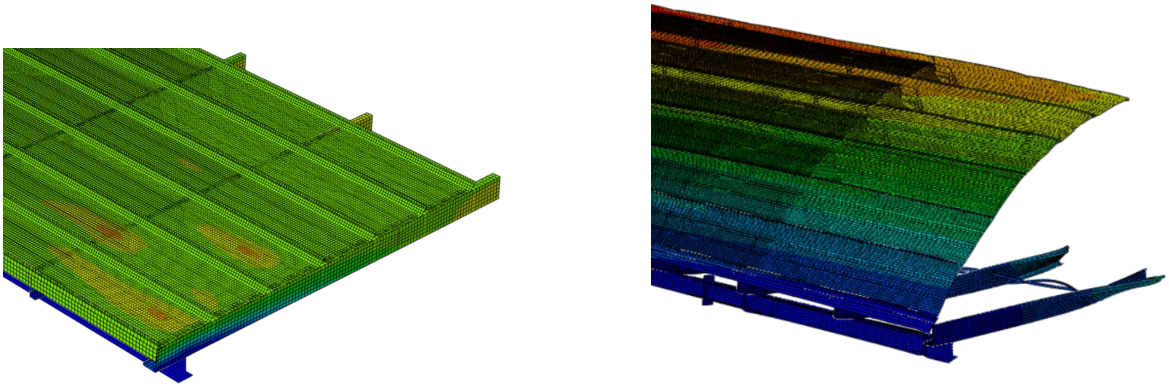

(a) 30 m/s (b) 70 m/s

Figure 5: Roof corner deformed shapes at low and high wind speeds

At 40 m/s, the main distinction among configurations (Table 1) is the spatial pattern of failed fasteners. Configurations 1 and 3 (Fig. 6a and Fig. 6b) show a more distributed failure pattern, with separated regions of eave screw failures and localized small groups of clip failures along multiple purlin lines. In contrast, Configurations 2 and 4 (Fig. 7a and Fig. 7b) show a more localized, clustered mechanism in which screw and clip failures concentrate into contiguous zones over a substantial portion of the corner panel. Configurations 2 and 4 exhibited comparable failure percentages that were approximately double the similarly aligned results of Configurations 1 and 3.

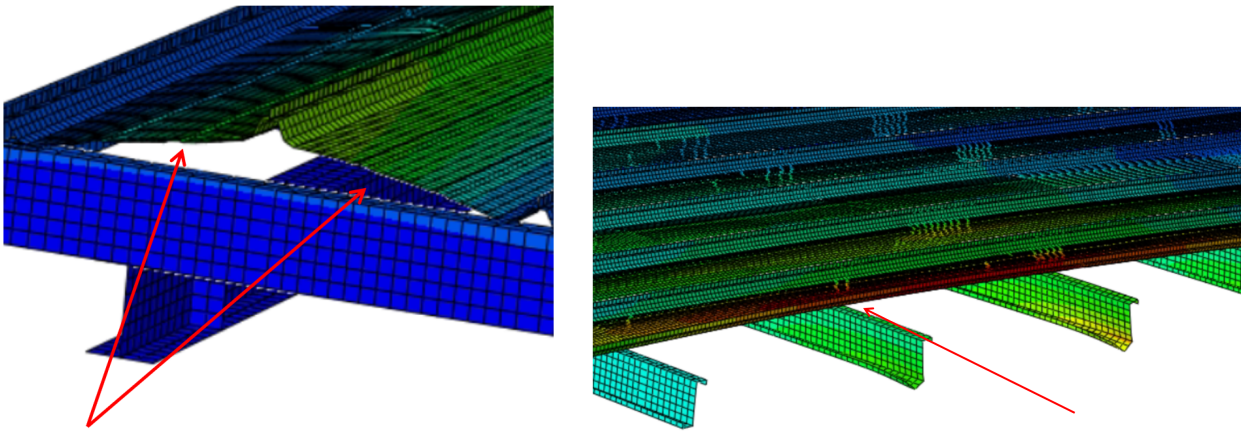

(a) Screw failure locations (b) Clip failure locations

Figure 6: Representative configurations 1 and 3 cases

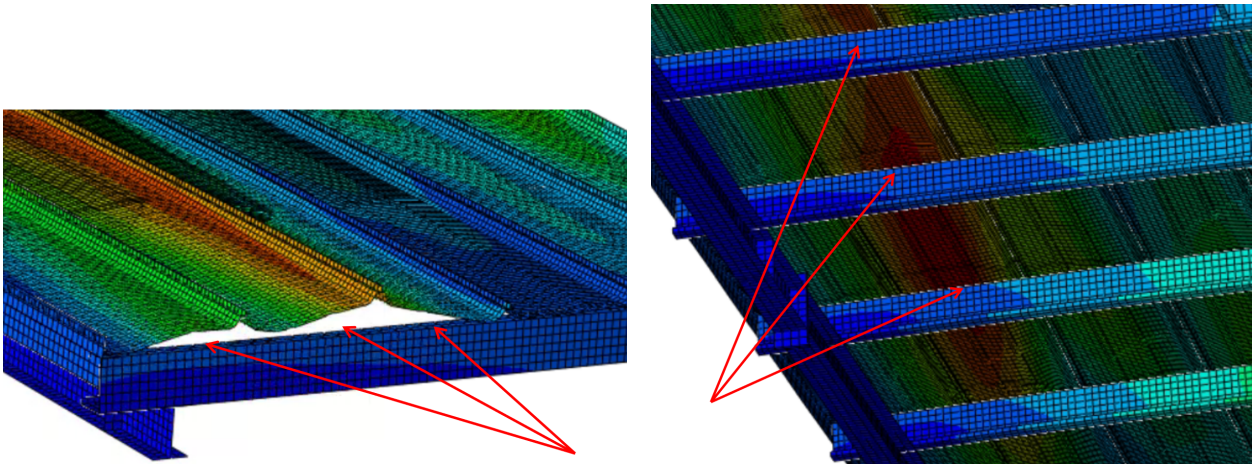

(a) Screw failure locations

(b) Clip failure locations

Figure 7: Representative configurations 2 and 4 cases

4.1 Failure progression and load path transition

Sequence plots show that, at the same reference wind speed, the order and location of fastener failures depend on the transient pressure history. Fig. 8 summarizes an example progression at 40 m/s in which clip failures initiate first. Early in the record (Fig. 8a), roof uplift is small and distributed, and the corner assembly remains well restrained.

As suction intensifies, clip failures initiate along the interior standing-seam lines, which reduces restraint between the roof panel and the purlins along those seams and allows larger deformation to develop (Fig. 8b). Once clips have failed in a local region, the remaining connectors carry a larger share of the uplift. As the tornado translates and the peak suction region moves toward the roof edge, failures extend to the eave screw line, and deformation becomes concentrated near the eave (Fig. 8c).

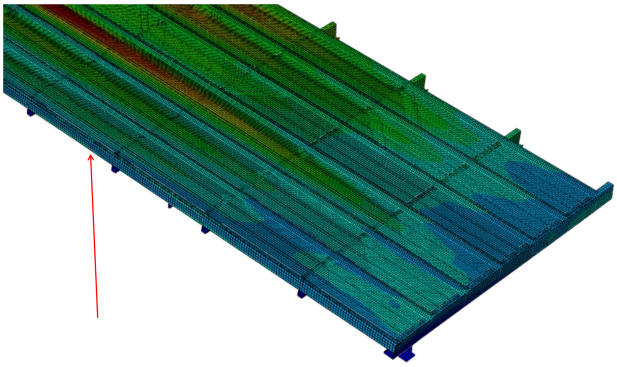

(a) Small distributed uplift

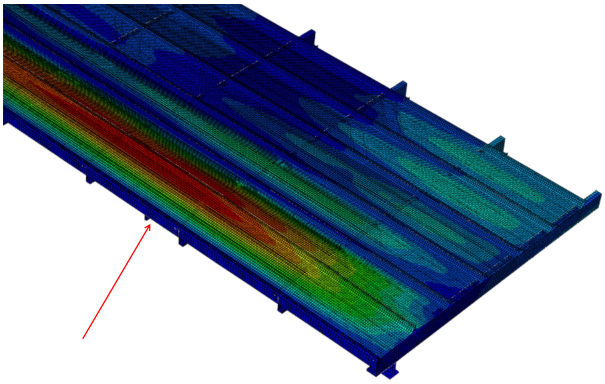

(b) Clip failure initiation

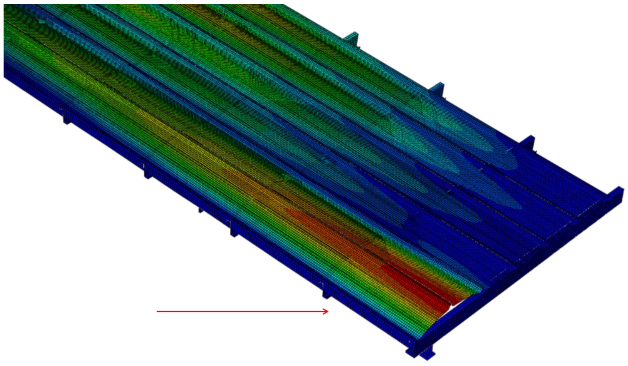

(c) Propagation to screws

Figure 8: Progression of roof panel uplift deformation with early clip failures

A complementary progression is also observed, in which eave screw failures initiate first and subsequently trigger clip failures. In this case, eave screw failures initiate early (Fig. 9a), producing roof panel edge separation and increased edge rotation (Fig. 9b). This early loss of edge attachment reduces the panel edge stability and promotes larger displacement, which trigger clip failures along interior purlins (Figs. 9c).

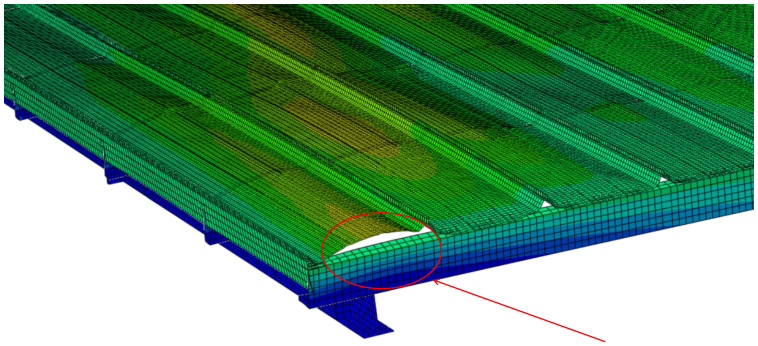

(a) Eave screw failure initiation

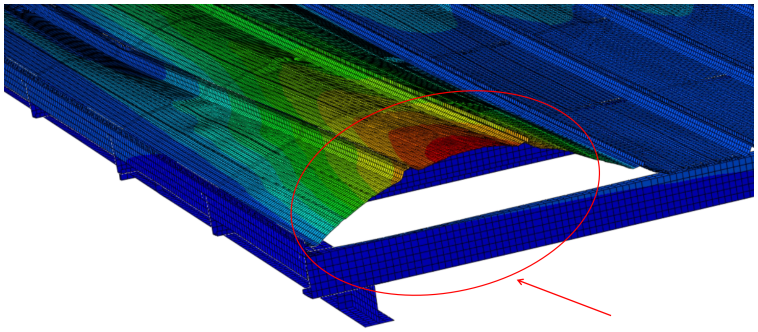

(b) Eave edge deformation

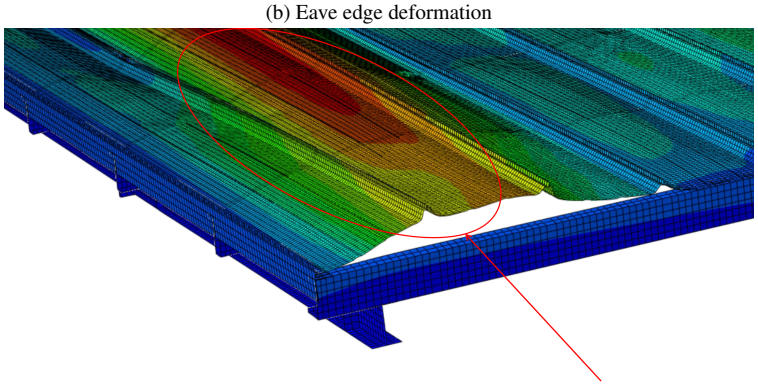

(c) Propagation to interior clips

Figure 9: Progression of roof panel uplift deformation with early screw failures

Another example is shown in Fig. 10, which illustrates one possible failure trajectory rather than a continuously propagating fastener failure. In this case, initial clip failures occur during an early suction peak (Fig. 10a). When the pressure temporarily drops, the connection failure is irreversible. Consequently, subsequent pressure peaks act upon a system with permanently compromised stability (Fig. 10b). These later peaks induce load redistribution around the damaged zone, concentrating forces onto adjacent intact fasteners and triggering secondary failures (Fig. 10c).

The key point is that, even at the same wind speed level, the transient pressure history can produce different sequences, either a more continuous spread of failures or an intermittent, peak triggered

cascade, yet both outcomes reflect the same stability mechanism: progressive connector loss reduces the effective panel to frame stiffness, promotes larger out-of-plane deformation and buckling, and increases force in the remaining fasteners during subsequent suction peaks.

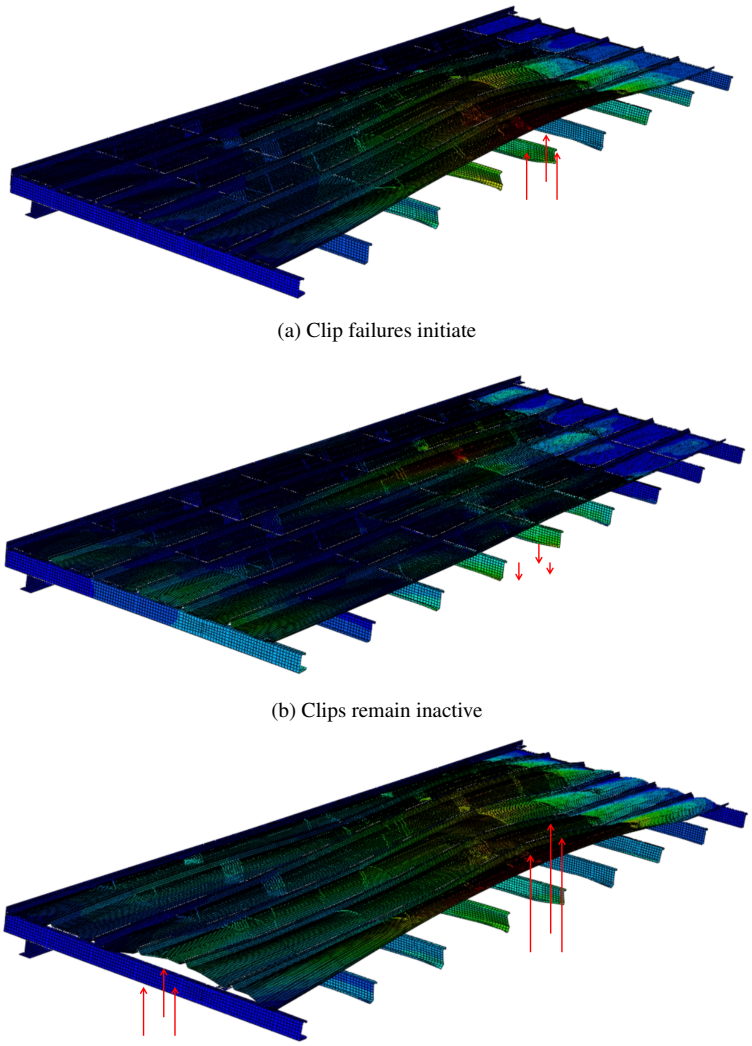

(a) Clip failures initiate

(b) Clips remain inactive

(c) Cascading failures expand

Figure 10: Early clip failure causes irreversible damage and later secondary fastener failures

5. Conclusions

This study developed a detailed finite element roof corner submodel in ABAQUS to evaluate roof corner response under tornado-induced external and internal pressures. The model extends the authors' prior one bay middle roof span framework by representing clips and eave screws as discrete connectors with pull-out and shear failure, which allows progressive fastener loss and the associated load redistribution to be captured. For each of the four configurations and five reference wind speeds, 25 finite element simulations were conducted using net pressure time history data from a tornado simulator to capture record to record loading variability. Roof corner response is summarized by the final percentage of failed fasteners and representative deformation with failure

plots. The failure percentages provide a probabilistic description of the structural response to loading variability, while the plots illustrate the associated localization of uplift and the progressive reduction in roof corner stability as connections fail under transient tornado pressures.

Reference wind speed controls the overall response. At 30 m/s, fastener failures are limited and roof deformation remains small. Conversely, at 50, 60, and 70 m/s, fastener failures propagate extensively across the corner region. Differences among internal pressure configurations are most clearly observed at 40 m/s. At this intermediate speed, the enclosed type scenarios (Configurations 1 and 3) exhibit a distributed failure pattern, whereas the opening type scenarios (Configurations 2 and 4) display dense failure clustering over a larger portion of the corner panel. Overall, the configurations featuring dominant openings yield significantly higher percentages of failed fasteners compared to the enclosed cases, demonstrates that the presence of a sustained opening compromises the structural stability of the roof corner, accelerating stiffness degradation and rendering the system vulnerable to widespread progressive failure.

Sequence plots show that, at the same reference wind speed, the order and location of fastener failures depend on the transient pressure history. As clips or eave screws fail, attachment stiffness decreases, roof deformation increases, and demand shifts to the remaining fasteners, which can trigger additional failures as the peak suction region moves across the roof corner.

Acknowledgments

This material is based upon work supported by the National Science Foundation under Grant Number 2053364. Any opinions, findings, and conclusions or recommendations expressed in this material are those of the author(s) and do not necessarily reflect the views of the National Science Foundation.

References

Abaqus (2016). *version 6.16*. Dassault Systèmes Simulia Corp.

Bajwa, Maninder Singh (2010). "Assessment of Analytical Procedures for designing metal buildings for Wind drift serviceability". PhD thesis. Virginia Tech.

Haan, Fred L., Vasanth Kumar Balaramudu, and Partha P. Sarkar (2010). "Tornado-Induced Wind Loads on a Low-Rise Building". *Journal of Structural Engineering*. ISSN: 0733-9445. DOI: 10.1061/(ASCE)ST.1943-541X.0000088.

Hong, Jong-Kook (2007). *Development of a seismic design procedure for metal building systems*. University of California, San Diego.

Kim, Yoon Duk (2010). *Behavior and design of metal building frames using general prismatic and web-tapered steel I-section members*. Georgia Institute of Technology.

Kopp, Gregory A. and C.-H. Wu (2020). "A framework to compare wind loads on low-rise buildings in tornadoes and atmospheric boundary layers". *Journal of Wind Engineering and Industrial Aerodynamics* 197. ISSN: 0167-6105. DOI: 10.1016/j.jweia.2020.104269.

Marshall, Timothy P. (2004). "Building damage issues in tornadoes". *22nd Conference on Severe Local Storms*. Paper P2.10. American Meteorological Society. Hyannis, Massachusetts, USA.

Niari, Shirin Esmaeili, Behzad Rafezy, and Karim Abedi (2015). "Seismic behavior of steel sheathed cold-formed steel shear wall: experimental investigation and numerical modeling". *Thin-Walled Structures* 96, pp. 337–347.

Roueche, David Brett, David O. Prevatt, and Frederick L. Haan (2020). "Tornado-Induced and Straight-Line Wind Loads on a Low-Rise Building With Consideration of Internal Pressure". *Frontiers in Built Environment* 6. ISSN: 2297-3362. DOI: 10.3389/fbuil.2020.00018.

Sengupta, Anindya et al. (2008). "Transient loads on buildings in microburst and tornado winds". *Journal of Wind Engineering and Industrial Aerodynamics* 96. ISSN: 0167-6105. DOI: 10.1016/j.jweia.2008.02.050.

SFS Group USA, Inc. (2024). *Roofing and Cladding Fastener Guide*. V1.02. RC 3022. SFS Group USA, Inc.

Sinno, R. Ralph (2005). "Simulation of Uplift Wind Loading on Metal Roofs Using Electromagnetic Suction Forces: Summary of Test Results". *MBMA Researchers' Symposium*. Metal Building Manufacturers Association. Atlanta, Georgia, USA.

Wang, Shihang et al. (2025). "Buckling behavior of metal building under dynamic wind loads". *Proceedings of the Annual Stability Conference*. SSRC Annual Stability Conference, April 2–4, 2025. Structural Stability Research Council. Louisville, Kentucky, USA.

Xia, Yuchao, Gregory A. Kopp, and Shuifu Chen (2023). "Failure mechanisms and load paths in a standing seam metal roof under extreme wind loads". *Engineering Structures* 296. ISSN: 0141-0296. DOI: 10.1016/j.engstruct.2023.116954.

Yu, Cheng and Benjamin W Schafer (2006). "Finite element modeling of cold-formed steel beams validation and application".